

1162 - 10007

NASA TN D-1108

NASA TN D-1108



TECHNICAL NOTE

D-1108

NONVISCIOUS FLOW THROUGH A PUMP IMPELLER ON A BLADE-
TO-BLADE SURFACE OF REVOLUTION

By James J. Kramer, Norbert O. Stockman, and Ralph J. Bean

Lewis Research Center
Cleveland, Ohio

NATIONAL AERONAUTICS AND SPACE ADMINISTRATION
WASHINGTON

February 1962

NATIONAL AERONAUTICS AND SPACE ADMINISTRATION

TECHNICAL NOTE D-1108

NONVISCIOUS FLOW THROUGH A PUMP IMPELLER ON A BLADE-
TO-BLADE SURFACE OF REVOLUTION

By James J. Kramer, Norbert O. Stockman, and Ralph J. Bean

SUMMARY

The nonviscous incompressible flow through a typical pump impeller is analyzed on a blade-to-blade surface of revolution. Solutions are obtained for a variety of inlet conditions including several with pre-whirl. The flow in the trailing-edge region is found to be a strong function of the assumed location of the rear stagnation point. Comparison of results from two approximate methods of analysis showed good agreement for the zero-angle-of-attack case and reliable indication of the existence of an eddy on the driving face at a large positive angle of attack.

INTRODUCTION

With the advent of large-thrust liquid-propellant rocket engines, high-performance liquid pumps became of considerable research interest. In order to take advantage of the gain in specific impulse associated with high combustion chamber pressure, high-pressure-rise pumps that are lightweight and efficient are required. Considerations of both low pump weight and high pump pressure rise point to high-rotative-speed pumps. The conventional cavitation limitations on suction specific speed, however, require such low pump speeds for good cavitation performance that pump weights would be prohibitive for advanced rocket propulsion systems. Hence, the suction specific speed limits must be raised. Increased suction specific speed limit implies that the fluid velocity distribution in the pump rotor must be carefully controlled.

High pump efficiency is required in order to maintain the number of pumping stages required at a minimum. Also, low-efficiency pumps require large turbine work outputs, which represent another rocket weight penalty. It has been shown in reference 1 that efficient centrifugal and mixed-flow air compressor performance can be attained by careful control of the fluid velocity distribution inside the impeller passages and that reliable design techniques can be developed for controlling the fluid velocity distribution. These design techniques are

based on potential flow models. Their development was based on insight gained into the flow process in impellers obtained from exact potential flow solutions (ref. 2).

No such solutions are available for impellers such as are commonly used in high-performance pumps for rocket propellant applications. In order to assist in the advancement of pump design technology, an analysis of the incompressible, nonviscous flow in a typical propellant pump rotor on a blade-to-blade surface of revolution using existing analytic techniques (ref. 3) was made. A typical mixed-flow axial-inlet pump impeller designed for rocket use is characterized by a high value of inlet blade angle (angle between axial direction and tangent to blade mean camber line). Large inlet angles result from the low values of axial velocity dictated by cavitation limitations and the high values of rotational speed required to produce large head rise per stage.

The analytic results presented herein are unique in that cases with nonzero prewhirl are treated. Pump inlet flows may have nonzero prewhirl where main pump stages are preceded by a rotating inducer stage or by stationary inlet guide vanes. Negative prewhirl (opposite to the direction of rotation) can be used to obtain increased head rise per stage. Positive prewhirl can be used to ease the problem of large inlet blade angles. The large inlet blade angles result in a limitation on the number of blades that can be used because of flow blockage effects. Imparting positive prewhirl to the fluid enables the designer to use smaller blade angles at zero angle of attack for the same volume flow rate as that without prewhirl, or to use the same blade angle at zero angle of attack for a lower volume flow rate.

This report presents the results of the analysis of the incompressible, nonviscous flow in a typical rocket pump impeller for a range of values of prewhirl and flow-rate parameters. These results consist primarily of flow velocities and slip factors. The blade surface velocity results are compared with those obtained from two rapid approximate methods of analysis. An investigation is made of the sensitivity of the exact solution results to the assumed location of the rear stagnation point.

ANALYSIS

The problem of analyzing the three-dimensional flow in a turbomachine is a formidable one. Because of practical computing limitations, the flow is usually analyzed in one of two mathematically two-dimensional surfaces: the blade-to-blade plane, or the meridional (hub-to-shroud) plane. The solutions obtained in the two planes are interrelated. The stream-sheet thickness variation obtained from a meridional-plane solution is required as input for a blade-to-blade solution. The mean flow

direction obtained from a blade-to-blade solution is required as input for a meridional-plane solution.

The solutions obtained in this report are on a blade-to-blade surface of revolution for an impeller designed by the method of reference 4. The impeller analyzed was one designed for a head rise of 2120 feet at a volume flow rate of 4.33 cubic feet per second and a rotative speed of 7600 rpm. The design method presented in reference 4 was carried out in the meridional plane to calculate streamline and velocity distributions for the hub shape, blade shape, and hub velocity distribution specified for the impeller. A meridional section of the impeller is shown in figure 1, and the specified blade shape is shown in figure 2. The impeller contains eight blades and has a design tip speed of 320 feet per second at the mean streamtube. The inlet and outlet blade angles are -83° and -41° , respectively.

A streamtube midway between the hub and shroud was selected for the blade-to-blade analysis. The streamtube geometry, which was held constant for all calculations, was obtained from the design calculations in the hub-shroud plane. Thus, the streamtube geometry used in the exact solution is a good approximation for flow conditions near those for which the hub-shroud design was carried out. However, at off-design flow conditions the streamtube geometry assumption becomes less valid. As a matter of convenience in the calculations, the streamtube geometry was approximated by analytic expressions.

The prescribed stream surface is a surface of revolution generated by a parabola through the blade row and outlet diffuser region and by an axial line tangent to the parabola upstream of the blade row. These curves are expressed analytically as follows:

$$\left. \begin{aligned} r &= 0.07465 z^2 + 0.1841 z + 3.1000 & \text{for } z \geq -1.2331 \\ r &= 2.9865 & \text{for } z < -1.2331 \end{aligned} \right\} \quad (1)$$

The graph of equation (1) is shown by the midline in figure 1.

The variation in radial stream-sheet thickness for the streamtube investigated (fig. 1) was prescribed as follows:

$$\left. \begin{aligned} b &= 0.004149 z^3 + 0.62314 z^2 - 0.319879 z + 0.596929 & \text{for } z \geq 3.75 \\ b &= \exp(-0.50852 z - 0.99571) & \text{for } 3.73 > z \geq 0.5 \\ b &= 0.000745 z^3 - 0.041216 z^2 - 0.105034 z + 0.349228 & \text{for } 0.5 > z \geq -1.2331 \\ b &= 0.4147 & \text{for } z < -1.2331 \end{aligned} \right\} \quad (2)$$

These equations are an approximation to the calculated middle streamtube thickness variation in the z-direction.

The partial differential equation describing the flow on a surface of revolution is derived in reference 5. For nonviscous incompressible flow, the equation becomes

$$\frac{1 + \lambda^2}{r^2} \frac{\partial^2 \psi}{\partial \theta^2} + \frac{\partial^2 \psi}{\partial z^2} + \left(\frac{\lambda}{r} - \frac{\partial \ln b}{\partial z} \right) \frac{\partial \psi}{\partial z} = 2\lambda\omega b \quad (3)$$

where ψ is defined by

$$\left. \begin{aligned} \frac{\partial \psi}{\partial z} &= -bw_\theta \\ \frac{\partial \psi}{\partial \theta} &= rbw_z \end{aligned} \right\} \quad (4)$$

(All symbols are defined in the appendix.) All derivatives with respect to z are along the stream surface; that is, these derivatives are the same as the bold-faced derivatives of reference 5.

In order to determine the flow through a pump impeller, a solution to equation (3) that satisfies the boundary conditions of the impeller must be found. A more complete discussion of the boundary conditions is given in reference 3, along with a method for obtaining the required solution to equation (3). Briefly, the method of reference 3 is to construct the solution for specified values of ω/V and prewhirl from certain basic solutions. The values of ω/V and prewhirl for the streamtube are specified through the parameters X and Y defined by the following equations:

$$X = \frac{\omega/V}{(\omega/V)_{\text{des}}}$$

$$Y = \frac{v_{\theta,u}}{\omega r_u}$$

For the streamtube analyzed, the value of $(\omega/V)_{\text{des}}$ is 7412 radians per cubic foot, and the value of ωr_u is 198 feet per second. The solutions for various operating conditions are dependent only on the ratios X and Y , and thus are independent of the magnitudes of ω , V , and $v_{\theta,u}$ as long as X and Y values are preserved.

The desired solution is expressed as a linear combination of the basic solutions; that is,

$$\psi = A_0\psi_0 + A_1\psi_1 + A_2\psi_2 + A_3\psi_3 \quad (5)$$

where the ψ_i are the basic solutions and Ψ is the desired solution satisfying specified boundary conditions. The basic solutions satisfy equation (3) and the boundary conditions shown in table I. The A_i values are obtained from the solution of four linear equations involving the A_i . These four equations are:

$$A_1 + A_2 + A_3 = 1.0 \quad (6)$$

$$A_0 = \frac{1}{\omega_0} \left(\frac{\omega}{V} \right) = \frac{1}{\omega_0} X \left(\frac{\omega}{V} \right)_{\text{des}} \quad (7)$$

$$\sum_{i=0}^3 A_i \left(\frac{\partial \psi_i}{\partial z} \right)_u = \frac{-b_u (v_{\theta, u} - \omega r_u)}{V} = b_u r_u X (1 - Y) \left(\frac{\omega}{V} \right)_{\text{des}} \quad (8)$$

$$\sum_{i=0}^3 A_i \left(\frac{\partial \psi_i}{\partial z} \right)_{\text{s.p.}} = 0 \quad (9)$$

Equation (6) specifies that Ψ varies from 0 to 1.0 across the flow passage. Equation (7) states that Ψ is the solution for the specified value of the parameter ω/V . Equation (8) specifies the ratio of upstream relative tangential fluid velocity to the volume flow rate. Equation (9) specifies the location of the rear stagnation point. Thus, solutions for any combination of prescribed values of the physical quantities X , Y , and location of the rear stagnation point can be obtained from linear combinations of the basic solutions. In all these solutions, Ψ will vary from 0 to 1 across the flow passage.

Numerical Procedure

The basic solutions were obtained by writing equation (3) in finite difference form using a grid of 863 points. The portion of the grid covering the rotor passage in the z - θ plane is shown in figure 2. The writing of equation (3) in finite difference form at each of the 863 interior grid points results in a set of 863 equations in 863 unknown ψ values (the values of ψ at the 863 interior grid points). These 863 equations were solved by using the extrapolated Gauss-Seidel iteration (ref. 6) on an IBM-650 digital computer. The extrapolated Gauss-Seidel iteration is a generalization of the ordinary Gauss-Seidel iteration; it involves an extrapolation parameter which, if chosen properly, speeds up the rate of convergence. One set of 863 equations had to be solved for each of the four basic solutions. Approximately 6 hours of machine time was required to obtain each of the basic solutions.

A three-point system was used for expressing the derivatives in finite difference form corresponding to approximating the unknown function by a second-degree polynomial in the neighborhood of the central grid point.

The accuracy of the various numerical techniques used in obtaining results is difficult to assess individually. Estimating the combined effect of inaccuracies at the various stages of the numerical procedure is even more formidable. The grid spacing data at the boundary points were known to be accurate to no more than two parts in the fourth decimal and only to about three places in the region of least accuracy. The Ψ values of the basic solutions were iterated until no changes occurred in the sixth decimal place in successive iterations at all 863 points. The overall result hoped for was Ψ values correct to three or four places and flow velocities (derivatives of Ψ) correct to within a few percent. This accuracy is more than adequate for engineering conclusions regarding the flow process.

15
10
5

Cases Considered

The specified conditions of the cases investigated are summarized in the first five columns of table II as values of X and Y and the resulting angle of attack α , mean inlet flow angle β_1 , and upstream relative velocity ratio $w_u/\omega r_t$.

The angle of attack is defined as the angle between the tangent to the blade mean line at the leading edge and the mean flow direction at the inlet to the blade row. The mean flow direction was computed by the one-dimensional continuity equation with the flow area based on blade blockage at $z = 0.08$ inch. At this point, the blade thickness in the θ -direction is 0.64 inch. The inlet stagnation point for this case occurs on the driving face at z equal to 0.035.

Case A represents the basic design condition with no prewhirl. Cases B, C, and D are corresponding off-design flows. Case E contains negative prewhirl, and cases F and G represent two flows with the same positive prewhirl. For cases A to G the stagnation point was assumed to occur at the blade tip, that is, the point on the blade with the maximum z coordinate. Case H is for the rear stagnation point location removed from the blade tip, as shown in the insert of figure 2. For case I, the slip factor rather than the stagnation-point location was prescribed.

RESULTS AND DISCUSSION

The results of the analysis are presented in four sections as:
(1) contour plots of stream function, velocity, and pressure for the

design case; (2) blade surface velocities for various off-design flow and prewhirl cases; (3) blade surface velocities for cases where the rear stagnation point is displaced from the tip; and (4) comparison of the results of the present analysis with approximate analysis methods (refs. 7 and 8).

Additional flow characteristics such as slip factor f_s , ratio of maximum relative blade surface velocity to relative upstream velocity w_{\max}/w_u , minimum pressure coefficient k defined as $(w_{\max}/w_u)^2 - 1$, head rise parameter ΔH defined as $\frac{H_o - H_i}{\omega^2 r_t^2 / g}$, and outlet flow angle

β_o were computed for each case. These computed values are listed in table II. The outlet station, denoted by subscript o , is at the tip of the blades, that is, at $z = 3.73$.

The slip factor f_s is defined as the ratio of the absolute tangential velocity of the fluid at the outlet of the blade row to the absolute tangential velocity that the fluid has if the outlet flow direction is assumed equal to the blade mean-line direction at the outlet. The calculated through-flow velocity decreases at the blade outlet because the blade thickness decreases from 0.157 inch to 0 as z increases from 3.70 to 3.73. In obtaining the denominator of f_s , the through-flow velocity was calculated from the flow area taking the blockage at $z = 3.70$ into account.

Design Case

Figures 3, 4, and 5 show streamlines, velocity contours, and pressure contours for design case A, for which ω/V equals 7412 radians per cubic foot and $v_{\theta,u}/\omega r_u$ equals 0 (no prewhirl). The angle of attack α is zero. The contour plots of figures 3, 4, and 5 are projections of the stream surface (a paraboloid of revolution) such that distances in the z and θ directions are invariant; angles are distorted. The tick marks at $\theta = 1.5$ indicate the line of no angular distortion. Angular distortion increases with distance from the tick marks.

The velocity contours of figure 4 are lines of constant ratio of the relative resultant fluid velocity to the tip speed of the impeller. With the velocities expressed in this ratio form, the values are independent of the value of ω when V is such that X is equal to 1.0, the value for case A. This figure shows an acceleration around the leading edge of the blade to a maximum velocity ratio greater than 0.80 on the trailing face. The velocity ratio then decreases to a value of approximately 0.45 and remains constant over a large portion of the mid-section of the blade. There is an acceleration and subsequent deceleration to the stagnation point in the trailing-edge region.

On the driving face of the blade the flow decelerates along the greater part of the blade surface until the acceleration and subsequent deceleration occur in the vicinity of the rear stagnation point. However, the grid in the leading- and trailing-edge regions was not sufficiently fine to indicate the shape of the contours between zero and 0.45 at the inlet and between zero and 0.30 at the outlet. The velocity becomes essentially uniform downstream of the blade row at a z distance from the blades equal to about four-tenths the distance between blades at the outlet. Upstream of the blade row, the velocity becomes essentially uniform at a z distance from the blade entrance equal to about eight-tenths the distance between blades at the inlet. These two stations are indicated by u and d in figure 1.

E-816

Figure 5 displays lines of constant static head parameter defined as the ratio $(h - h_u)/(\omega^2 r_t^2/2g)$. Again, these contours are independent of the value of ω when V is such that X is equal to 1.0. The cavitation problem in liquid pumps is demonstrated by the region of negative values of static head parameter. The minimum value of head parameter attained is -0.27 (as indicated in fig. 5) corresponding, for example, to a depression in static head of 430 feet at the design tip speed of 320 feet per second.

Off-Design Cases

Effects of angle of attack. - Blade surface velocities are presented in figure 6 for a range of angle of attack from $-1^\circ 44'$ to $5^\circ 9'$ with no prewhirl (cases A to D). The relative resultant velocity ratio is plotted against the distance ratio s , where s is the fraction of the total distance along the blade surface from the intersection of the mean camber line and the leading edge to its intersection with the trailing edge. For all the cases shown in figure 6, the rear stagnation point was assumed to occur at the blade tip.

Figure 6 shows the velocity peaks in the leading- and trailing-edge regions caused by the extreme local blade curvature in these regions. Whether the velocity peaks near the trailing edge will occur in the flow of a real fluid is open to serious question, because the potential flow model is not expected to produce a good approximation to the real fluid flow (wake formation) in this region.

In the leading-edge region, the maximum trailing surface velocity increases and the maximum driving surface velocity decreases as the angle of attack increases and shifts the inlet stagnation point toward the driving surface. This result is similar to the condition that exists for airfoils. The driving surface velocity decreases over most of the surface, while the trailing surface velocity decreases more rapidly in the inlet region.

Examination of the velocity variations of figure 6 indicates consistently high loading in the outlet region. The blade loading in the inlet region increases with increasing angle of attack. For case D, the through-flow velocity is sufficiently low and the loading sufficiently high that an eddy is formed on the driving surface of the blade as evidenced by the negative velocities.

The slip factor decreases slightly as angle of attack increases. For fixed tip speed and no prewhirl, the angle of attack is increased by decreasing the through-flow velocity. Consequently, if f_s remains constant, the outlet absolute tangential velocity will be increased for a backward swept blade, which results in an increase in head rise as α increases. The result can be noted in table II.

Effects of prewhirl. - The surface velocity variations for a case with negative prewhirl (case E) are shown in figure 7(a), and for two cases with positive prewhirl (cases F and G) in 7(b) and (c). Negative prewhirl (case E) results in a higher head rise at the same tip speed than the no-prewhirl case for the same flow rate (case A). The change in blade velocity distribution occurs over the initial 10 percent of the driving face and 30 percent of the trailing face. The velocity variation in the leading-edge region is similar to that for case C, which has nearly the same α as case E. However, the peak blade surface velocity is higher for case E because of its smaller value of X , which indicates a higher flow rate at the same rotative speed.

Positive prewhirl (cases F and G) results in a lower head rise than a case with no prewhirl at the same tip speed. Again, the resultant change in blade loading is restricted to the inlet region. Also, peak surface velocities are lower for cases with the same α (cases B and A) because of the higher values of X (lower flow rate at same rotative speed).

Inspection of table II reveals that cases with the same value of X and different α (caused by differing prewhirl) have the same value of f_s . Thus, f_s appears to be a function primarily of X . However, the total variation in f_s over the range of cases investigated is slight.

Design Uses of Results

The detailed knowledge of flow conditions inside pump impellers is useful to a designer in two important respects: pump efficiency and cavitation performance. The blade surface velocities determine the boundary-layer growth and thus strongly influence pump efficiency. Unfortunately, no correlating parameter has been developed for relating pump efficiency to blade surface velocities. Thus, no means are at hand for comparing quantitatively the cases considered from the standpoint of pump efficiency.

The cavitation performance of a pump is determined by the region of low static head near the blade leading edge. A parameter frequently used for comparing blade cavitation performance is the minimum pressure coefficient k defined as $(w_{\max}/w_u)^2 - 1$. The values of k have been computed for the cases considered and are listed in table II. The minimum value of k for these cases occurs for case B, where the blade operates at a small negative angle of attack. These results indicate that the blade would operate cavitation-free at a lower value of net positive suction head for the same rotative speed at a small negative α than at zero α . This holds even though the flow rate is higher at a negative α than at zero α for the same rotative speed. These results, however, are not completely comparable in that the change in α is effected by a change in X , which also results in a change in static head rise parameter. Thus, for the same rotative speed for both cases A and B, case A has a lower flow rate and a higher head rise across the rotor than case B.

Among the cases with prewhirl, case F has the lowest value of k . Again, case F has a small negative α . However, comparison of the various cases for design purposes is hindered by differing head rise parameters. The comparison considerations are further complicated by the question of how the prewhirl is generated. If the prewhirl is generated by stationary inlet guide vanes, then no work is done on the fluid, and upstream tangential velocity is generated at the expense of static head. If a rotating inducer is used, the possibility of pressure rise across the inducer is introduced, and cavitation considerations are considerably more complicated.

The calculated results presented in this report will not materially assist the designer in the selection of blade shape and operating conditions, since only one blade shape has been investigated for several operating conditions. The results presented herein have their utility in indicating how the flow in a typical blade varies over a range of operating conditions. Thus, these results assist the designer in estimating off-design performance.

The investigation of the analysis method itself is important to the designer. The analysis method used herein is the most exact means available for determining the flow in a pump impeller. The capability of determining the flow in a particular impeller is useful to the designer in screening tentative designs. The knowledge of the limitations of an analysis method is vital to intelligent use of that method. Similarly, the knowledge of the validity of approximate methods gained by comparison with a more exact method is necessary for the confident use of these approximate methods. These two areas of interest are discussed in the following two sections.

Effects of Rear Stagnation Point Assumption

For all the results presented thus far, the rear stagnation point was assumed to occur at the blade tip, point A in figure 2. In order to investigate the effect of this assumption on the results, case H was constructed, in which the rear stagnation point was assumed to occur at the point labeled H in figure 2. It was convenient to choose the location of the rear stagnation point as shown because a grid point in the original grid of the problem occurred there. Thus, it was easy to specify the value of the derivative of Ψ with respect to z at that point. For case H, the parameter X is equal to 1.0 and Y is equal to 0, the same values as for case A.

The blade surface velocities for cases A and H are shown in figure 8. The velocities do not differ upstream of s equal to 0.61 on the driving face or upstream of s equal to 0.87 on the trailing face. These two s locations are the intercepts of the blade surfaces and a line normal to the mean flow direction. The differences in velocity distribution between cases A and H indicate an increase in blade loading in the trailing-edge region accompanied by an increase in f_s from 0.84 for case A to 0.98 for case H.

These results suggest an alternative way of specifying the A_i used in constructing the real solutions. Instead of the equation specifying the location of the rear stagnation point (eq. (9)), an equation specifying the downstream tangential velocity could be used; that is,

$$\sum_{i=0}^3 A_i \left(\frac{\partial \psi_i}{\partial z} \right)_d = \frac{-b_d (v_{\theta,d} - \omega r_d)}{V} \quad (10)$$

Equation (10) was used with equations (6), (7), and (8) to construct case I, in which the downstream tangential velocity was specified such that the slip factor f_s was equal to 0.91. The quantities X and Y were specified equal to 1.0 and 0, respectively. The blade surface velocities for case I are also shown in figure 8. The velocity profile is similar in shape to that for cases A and H. Deviation of case I from case A begins at the same point as for case H. However, the increase in trailing-edge blade loading for case I is not as great as for case H because f_s is lower.

The sensitivity of the solution to changes in the location of the rear stagnation point is demonstrated by figure 8. The shapes of the curves in the figure are consistent, and the curves do not differ at all until the flow has traversed from 61 to 87 percent of its path length through the impeller. Therefore, the conclusions concerning the flow over the forward part of the blade (e.g., those concerning the effect of α) are probably valid in spite of the uncertainty in the location of the rear stagnation point.

The changes in blade surface velocities brought about by changes in rear stagnation point location indicate nothing about the actual operation of such an impeller. In the flow of a real fluid through such an impeller, the formation of wakes at the blade trailing edge will result in a quite different flow distribution near the trailing edge. This is a general limitation of potential flow analyses that should be remembered when these results are being used. The present results indicate that f_s and ΔH are strongly dependent on the trailing-edge flow. As a result, this potential flow analysis gives no reliable information on these parameters.

Previous work in the field of potential flow analysis (refs. 9 and 10) is based on assuming the location of the stagnation point. Reference 9 assumes that the stagnation point occurs at the blade tip for non-cuspidate pointed blades and at the intersection of the mean camber line and blade surface for somewhat rounded blades. Reference 10 states that for rounded blades either the position of the stagnation point can be assumed or some available empirical rules for the exit angle used. In view of the sensitivity of certain aspects of the flow to the location of the stagnation point, specification of the rear stagnation point is an area requiring further work. Until more information is obtained concerning this matter, the use of some empirical rules for f_s or, equivalently, outlet flow angle appears to be a more practical course.

Comparison with Approximate Methods

Two approximate methods for predicting blade surface velocities have been developed and are reported in references 7 and 8. These two methods, the circulation method and linear pressure method, differ primarily in the simplifying assumptions made. In the circulation method, the flow direction is given by the average of the blade driving and trailing surface directions except near the outlet, where the effect of slip has been taken into account. Near the leading edge, both the blade surface angles were assumed equal to the mean-line angle. Also, in the circulation method the mean flow velocity computed using one-dimensional continuity considerations is assumed to be the arithmetic average of the blade surface velocities.

In the linear pressure method the flow direction is assumed equal to the direction of blade mean camber line except near the outlet, where slip is considered. In place of the velocity assumption in the circulation method, an assumption is made concerning the pressure in the linear pressure method. That assumption is that the mean pressure computed using one-dimensional flow relations is assumed to be the arithmetic average of the blade surface pressures.

For both methods the effect of slip was taken into account as follows: The flow direction at the outlet of the blade row was computed

for an assumed slip factor. A parabolic variation in flow direction was then prescribed between the point where slip begins to occur, R_x , and the blade row outlet.

Calculations of blade surface velocities were made for cases A ($\alpha = 0^\circ$) and D ($\alpha = 5^\circ 9'$) by the circulation and linear pressure methods. Calculations were begun at $z = 0.025$. Upstream of that point, a flow channel was difficult to define. For these calculations the value of f_s was taken from the exact solutions, and the value of R_x was obtained from the empirical relation given in reference 7.

The results of the circulation and linear pressure methods for the same conditions as specified for case A are shown in figure 9. The agreement of both approximate methods with the exact solution for case A is good on the driving face and on most of the trailing face. The good agreement at the condition for α equal to zero indicates the considerable value of these methods as a guide in impeller design.

In the design of rotors using reference 4, in which blade surface velocities are calculated by the linear pressure approximate method, a region in which the static pressure is greater than the total pressure on the driving face frequently has been encountered in instances of relatively high blade loading at low flow rates. Calculation of the flow velocities results in imaginary values. These results have been interpreted as indicating negative flow velocities, that is, an eddy on the driving face of the blade. In order to check this interpretation, the results of the approximate methods were compared with the exact results for case D in figure 10. This comparison indicates that the region interpreted as indicative of negative velocities does correspond to the eddy on the driving face of the blade. However, the linear pressure method exaggerates the magnitude of the negative velocities, whereas the linear velocity method underestimates this effect. Because impellers are designed to avoid this eddy condition by some margin in order to insure reasonable off-design performance, the indication of the existence of the eddy by the approximate methods should be adequate to warn the designer of an unacceptable flow condition.

Near the outlet and inlet, neither method yielded good agreement with the exact solution. The flow around the leading and trailing edges is strongly influenced by the local shape of the blade rather than by channel flow processes in which the flow is determined primarily by the gross geometry of the flow passage between blades. Thus, the approximate methods are of quite limited value in studying cavitation conditions.

SUMMARY OF RESULTS

The results of the analysis of the blade-to-blade flow through a typical pump impeller can be grouped into three general areas as follows:

1. Velocity distributions were obtained for a range of operating conditions including cases with prewhirl. The effects on the velocity distribution caused by varying angle of attack with a fixed flow rate are confined to the initial 30 percent of the trailing face and 10 percent of the driving face. As the angle of attack is increased, the maximum trailing surface velocity increases. The smallest value of minimum pressure coefficient was obtained at a small negative angle of attack. The negative angle of attack implies a lower head rise and a higher flow rate than the zero-angle-of-attack condition at the same rotative speed. The slip factor was essentially constant over the range of cases investigated. These results were obtained with the rear stagnation point fixed at the blade tip.

2. Moving the rear stagnation point slightly caused a marked change in the trailing-edge velocity distribution, which resulted in a large change in slip factor. Because of this, the calculated slip factors and head rise parameters are of uncertain value. The flow over the major part of the blade surface was unaffected, so that conclusions regarding the inlet flow are valid. It appears that specification of slip factor by some empirical data is more useful than specification of the rear stagnation point.

3. Both approximate methods of analysis gave about the same good agreement with the exact solution for the zero-angle-of-attack case. The agreement with the exact results was poor for the off-design case investigated (5° angle of attack) in the leading- and trailing-edge regions. However, the approximate methods were adequate to predict the presence of the eddy on the driving face.

Lewis Research Center

National Aeronautics and Space Administration
Cleveland, Ohio, September 5, 1961

APPENDIX - SYMBOLS

The following symbols are used in this report:

A	coefficient of basic solution in linear combination
b	stream-sheet thickness in radial direction, in.
f_s	slip factor
g	acceleration due to gravity
H	total head
ΔH	head rise parameter, $\frac{H_0 - H_1}{(\omega r_t)^2/g}$
h	fluid static head
k	minimum pressure coefficient, $\left(\frac{w_{max}}{w_u}\right)^2 - 1$
R_x	radius at which fluid is no longer considered to be perfectly guided by the blades
r	radial distance from impeller axis, in.
s	fraction of total distance along blade surface from leading edge to rear stagnation point
V	volume flow rate through streamtube
v	absolute fluid velocity
w	fluid velocity relative to rotating impeller
X	parameter indicating fraction of design ratio of rotor angular velocity to volume flow, $\frac{\omega}{V}/\left(\frac{\omega}{V}\right)_{des}$
Y	prewhirl parameter, $v_{\theta,u}/\omega r_u$
z	axial distance from impeller inlet, in.
α	angle of attack, deg
β	mean flow angle, deg
θ	angular distance from an arbitrary radial line, radians

λ	dr/dz
Ψ	stream function for real solution defined by eq. (5)
ψ	stream function for basic solution defined by eq. (4)
ω	rotor angular velocity, radians/sec

Subscripts:

d	downstream (fig. 1)
des	design
i	blade inlet
i, 0, 1, 2, 3	basic solution numbers
max	maximum value on blade surface
o	blade outlet
s.p.	stagnation point
t	impeller tip
u	upstream (fig. 1)
z	component in z-direction
θ	component in θ -direction

REFERENCES

1. Kramer, James J., Osborn, Walter M., and Hamrick, Joseph T.: Design and Test of Mixed-Flow and Centrifugal Impellers. Trans. ASME, Jour. Eng. for Power, ser. A, vol. 82, Apr. 1960, pp. 127-135.
2. Stanitz, J. D.: Some Theoretical Aerodynamic Investigations of Impellers in Radial- and Mixed-Flow Centrifugal Compressors. Trans. ASME, vol. 74, no. 4, May 1952, pp. 473-497.
3. Kramer, J. J.: Analysis of Incompressible, Nonviscous Blade-to-Blade Flow in Rotating Blade Rows. Trans. ASME, vol. 80, no. 1, Jan. 1958, pp. 263-275.
4. Smith, Kenneth J., and Hamrick, Joseph T.: A Rapid Approximate Method for the Design of Hub Shroud Profiles of Centrifugal Impellers of Given Blade Shape. NACA TN 3399, 1955.

5. Wu, Chung-Hua: A General Theory of Three-Dimensional Flow in Subsonic and Supersonic Turbomachines of Axial-, Radial-, and Mixed-Flow Types. NACA TN 2604, 1952.
6. Kahan, William M.: Gauss-Seidel Methods of Solving Large Systems of Linear Equations. Ph.D. Thesis, Univ. of Toronto, 1958.
7. Stanitz, John D., and Prian, Vasily D.: A Rapid Approximate Method for Determining Velocity Distribution on Impeller Blades of Centrifugal Compressors. NACA TN 2421, 1951.
8. Hamrick, Joseph T., Ginsburg, Ambrose, and Osborn, Walter M.: Method of Analysis for Compressible Flow Through Mixed-Flow Centrifugal Impellers of Arbitrary Design. NACA Rep. 1082, 1952. (Supersedes NACA TN 2165.)
9. Stanitz, John D.: Two-Dimensional Compressible Flow in Turbomachines with Conic Flow Surfaces. NACA Rep. 935, 1949. (Supersedes NACA TN 1744.)
10. Wu, Chung-Hua, and Brown, Curtis A.: Method of Analysis for Compressible Flow Past Arbitrary Turbomachine Blades on General Surface of Revolution. NACA TN 2407, 1951.

TABLE I. - BOUNDARY VALUES FOR BASIC SOLUTIONS

Basic solution	Boundary value of ψ						ω
	At A	At D	At E	At H	Along BC	Along FG	
0	0	0	0	0	0	0	ω_0
1	0	0	1	1	0	1	0
2	0	1	2	1	0	1	0
3	1	0	1	2	0	1	0

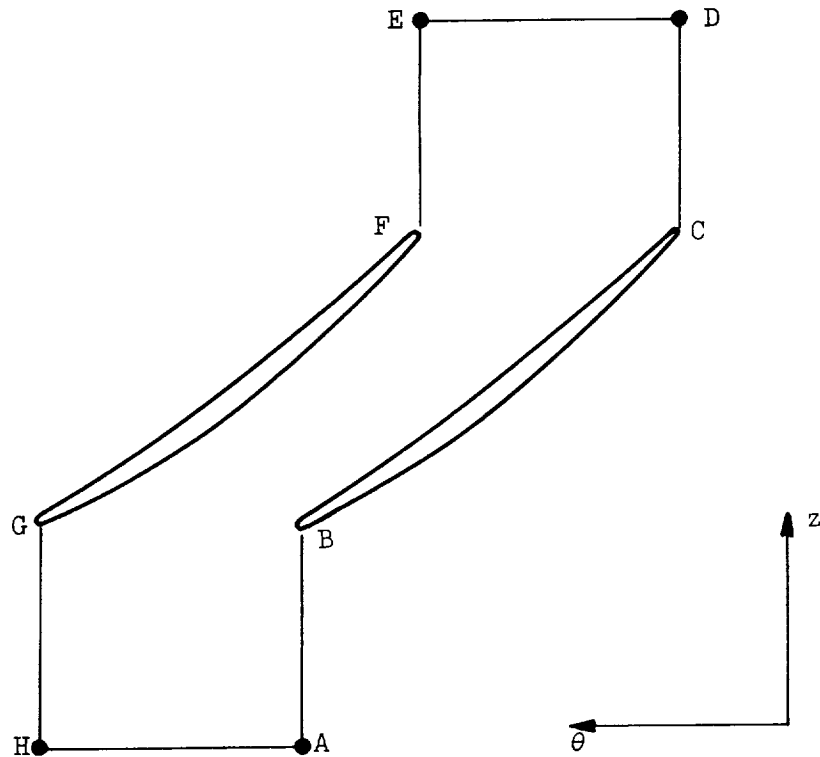


TABLE II. - SUMMARY OF SPECIFIED CONDITIONS AND RESULTANT FLOW PROPERTIES

Case	X	Y	α	β_i	$\frac{w_u}{\omega r_t}$	f_s	$\frac{w_{max}}{w_u}$	k	ΔH	β_o
A	1.0	0	0°	-83°4'	0.62	0.84	1.34	0.80	0.623	-51°37'
B	.8	0	-1°44'	-81°20'	.62	.85	1.21	.46	.571	-48°58'
C	1.33	0	1°43'	-84°47'	.62	.84	1.47	1.16	.675	-55°27'
D	4.0	0	5°9'	-88°15'	.62	.83	1.63	1.66	.780	-71°17'
E	1.0	-.333	1°37'	-84°41'	.83	.84	1.42	1.02	.751	-51°57'
F	1.0	.2	-1°35'	-81°29'	.50	.84	1.24	.54	.547	-51°37'
G	1.25	.2	0°6'	-83°10'	.50	.84	1.36	.85	.588	-54°32'
H	1.0	0	0°	-83°4'	.62	.98	1.34	.80	.726	-42°29'
I	1.0	0	0°	-83°4'	.62	^a .91	1.34	.80	.675	-47°26'

^aValue specified for calculation.

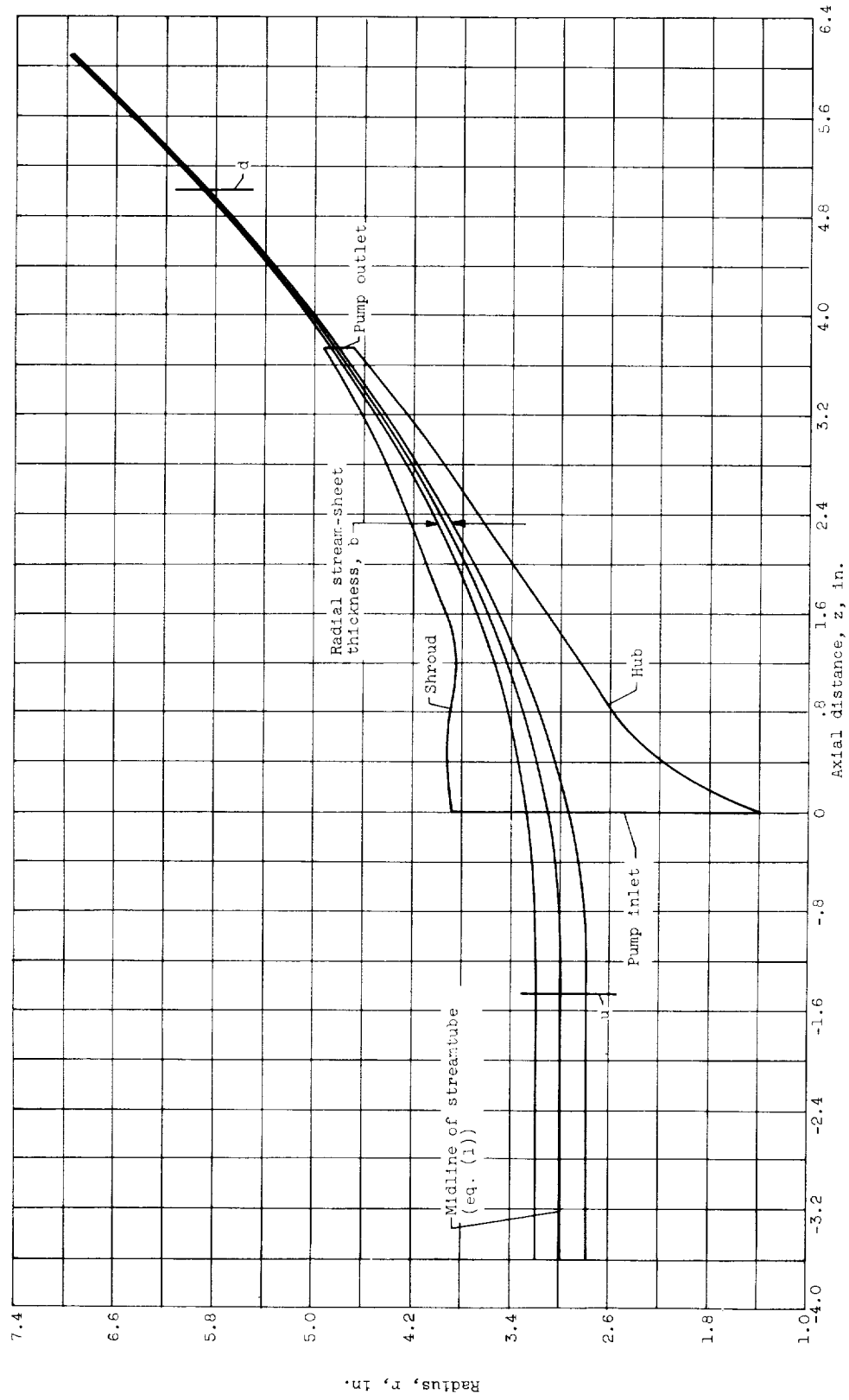


Figure 1. - Hub-shroud profile of pump showing meridional section of streamtube analyzed in this report.

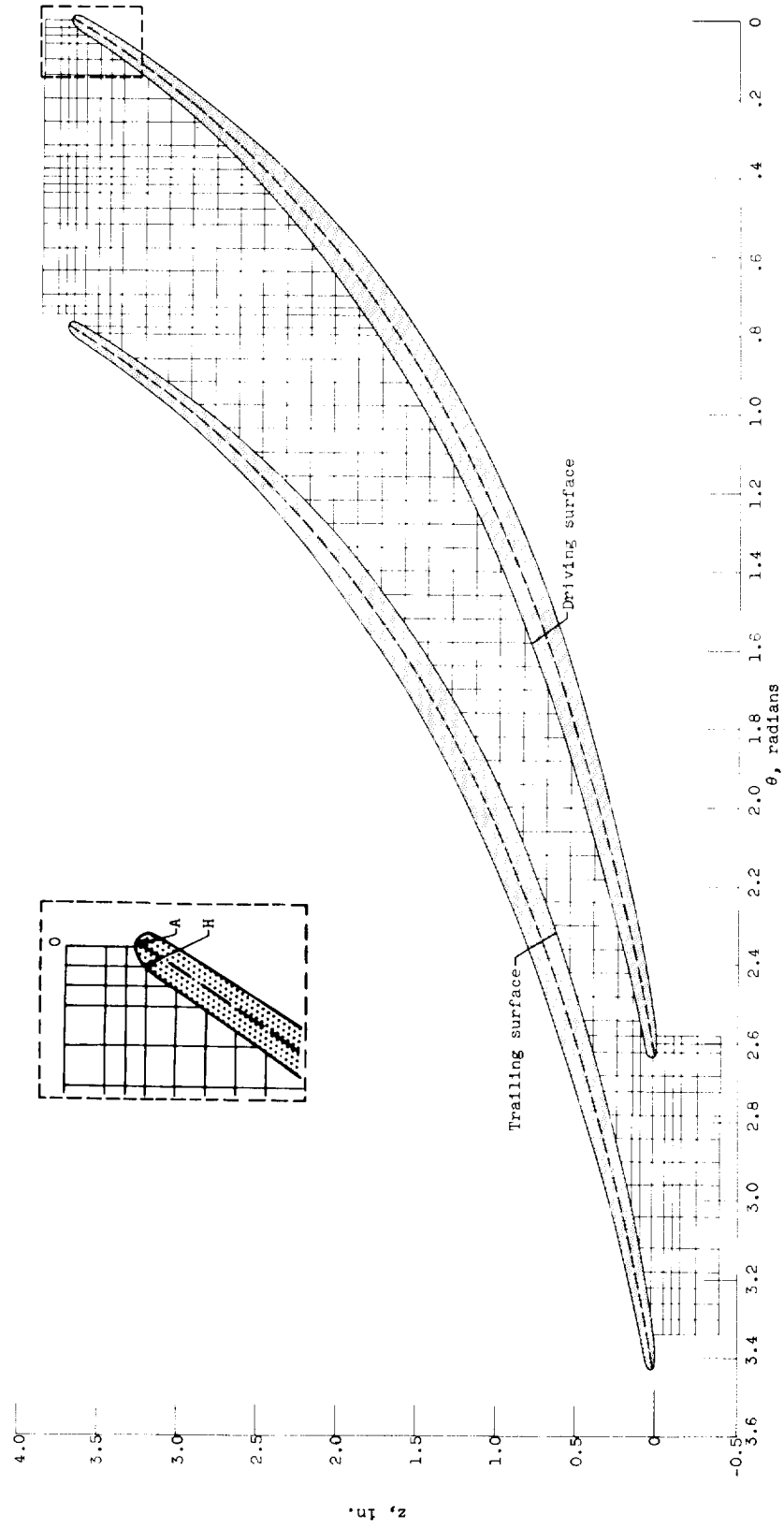


Figure 2. - Blade-to-blade view of streamtube showing grid used for numerical solution.

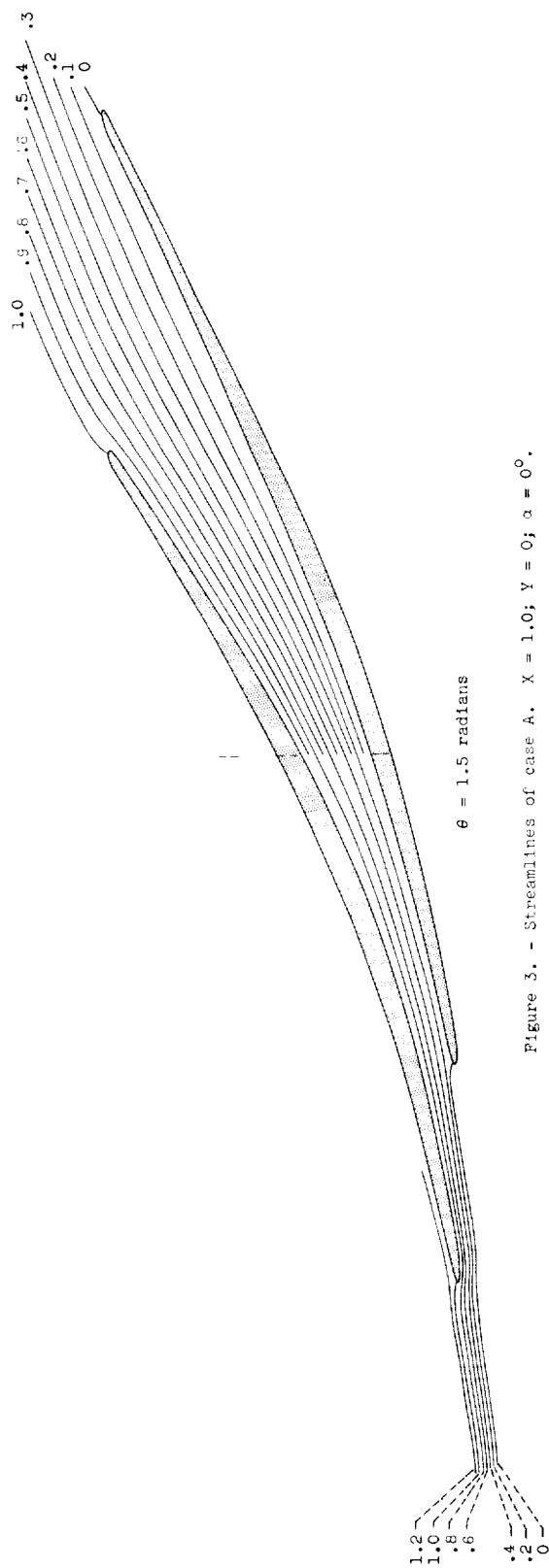


Figure 3. - Streamlines of case A. $X = 1.0$; $Y = 0$; $\alpha = 0^\circ$.

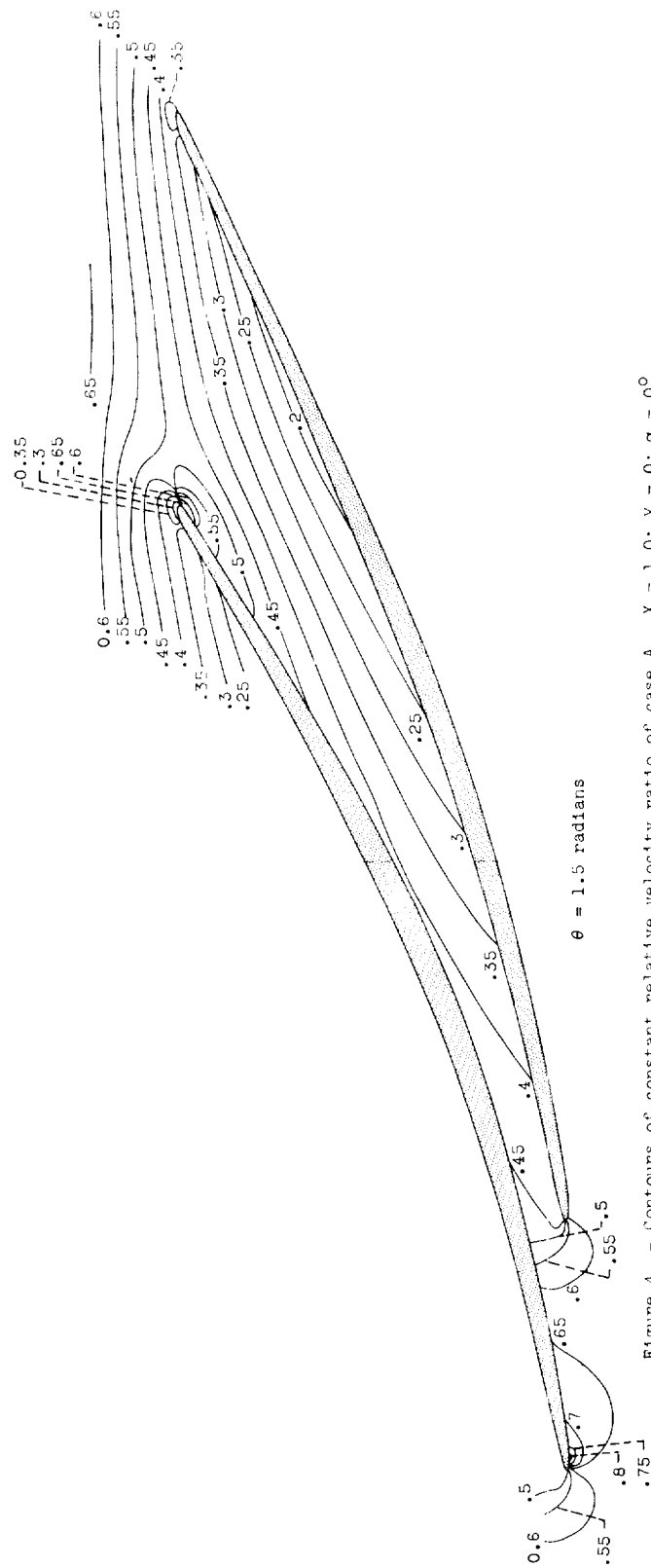


Figure 4. - Contours of constant relative velocity ratio of case A. $X = 1.0$; $Y = 0$; $\alpha = 0^\circ$.

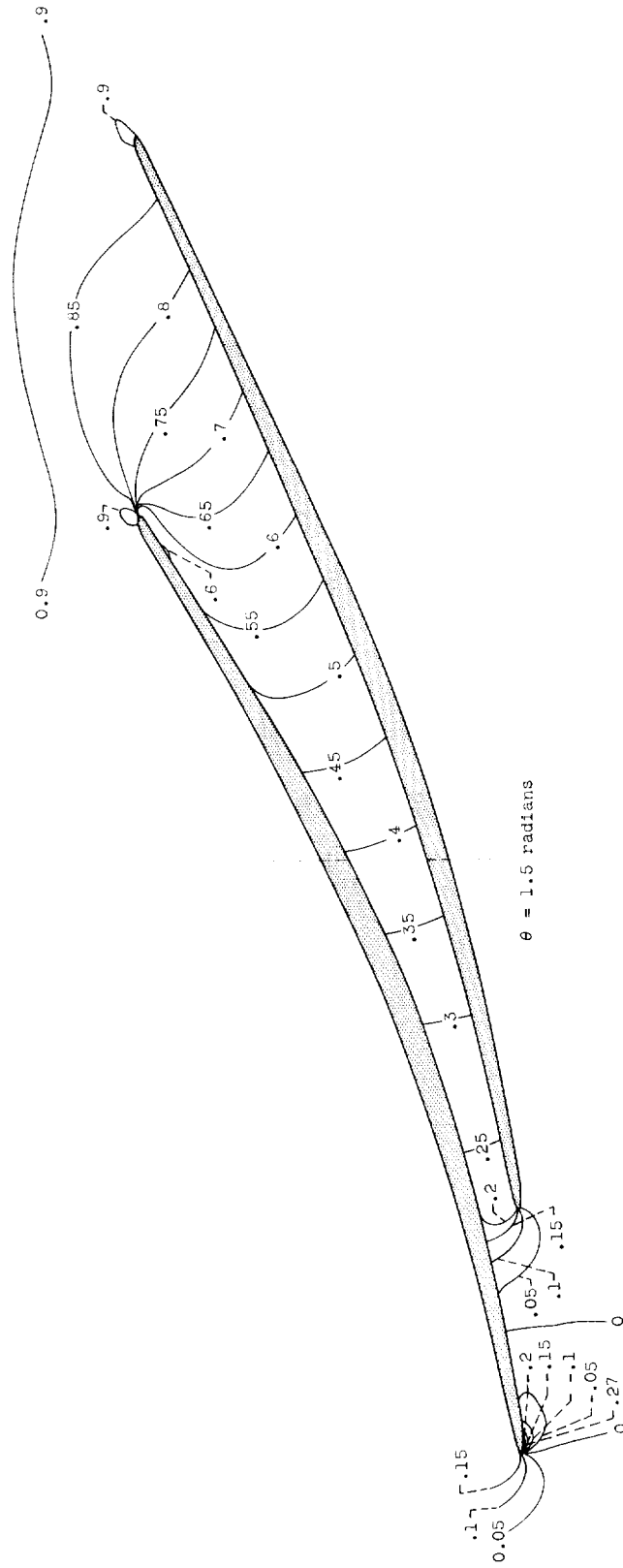


Figure 5. - Contours of constant static head parameter of case A. $X = 1.0$; $Y = 0$; $\alpha = 0^\circ$.

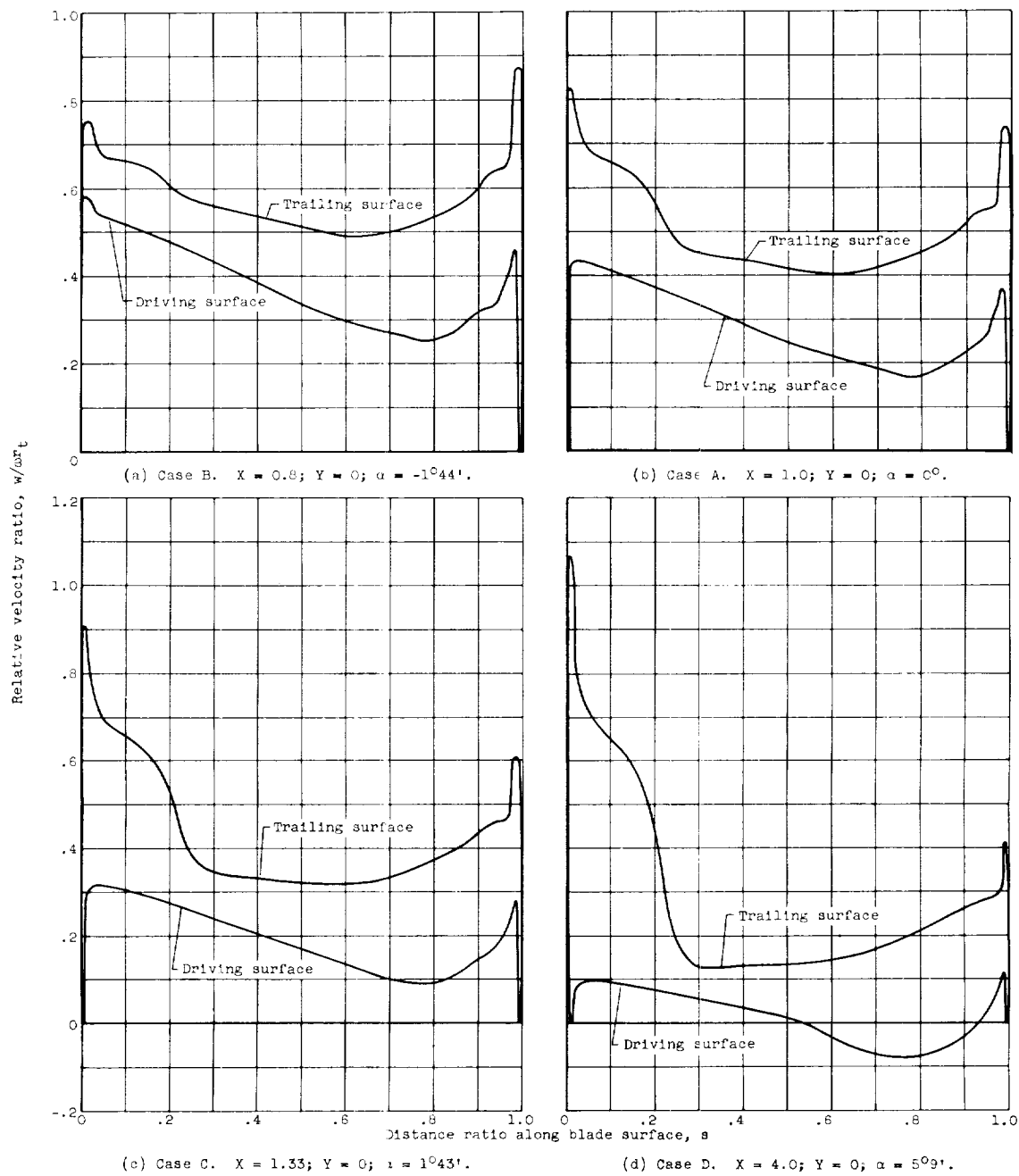


Figure 6. - Distribution of relative velocity ratio along blade surfaces for varying angle of attack, zero prewhirl, and rear stagnation point at tip.

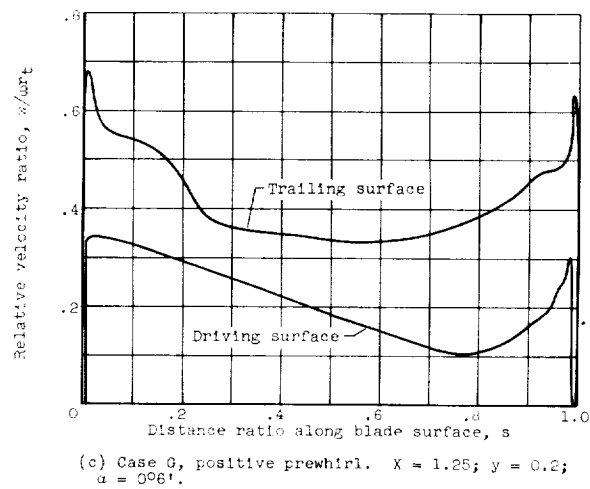
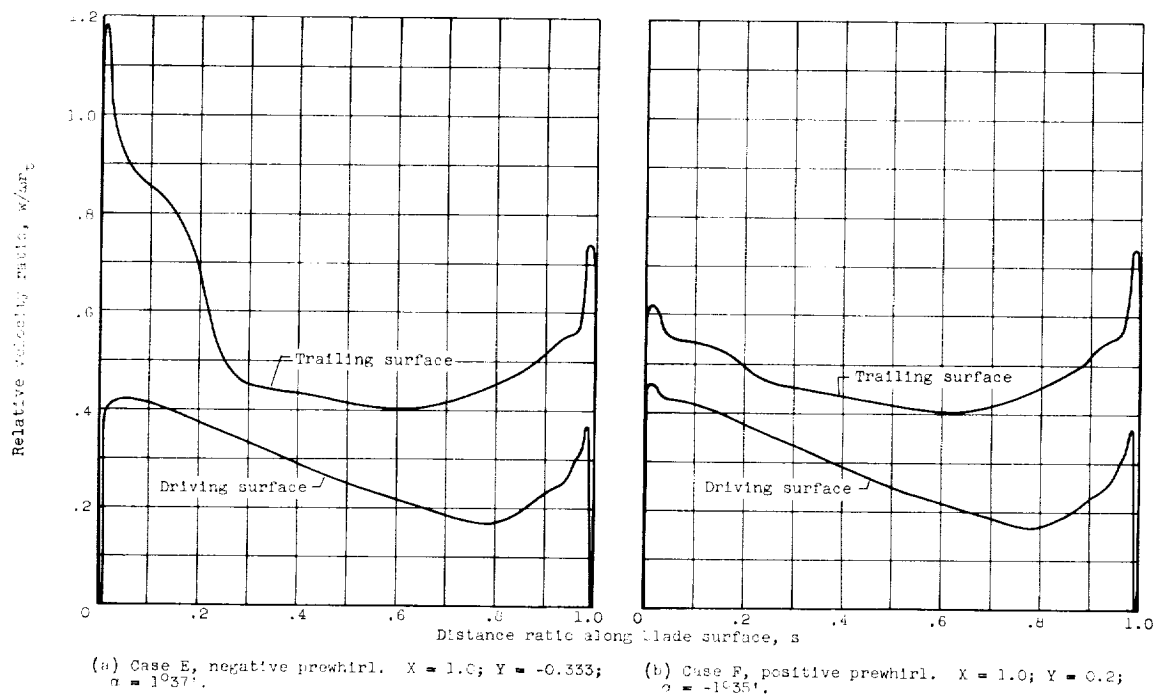


Figure 7. - Distribution of relative velocity ratio along blade surfaces for cases with prewhirl.

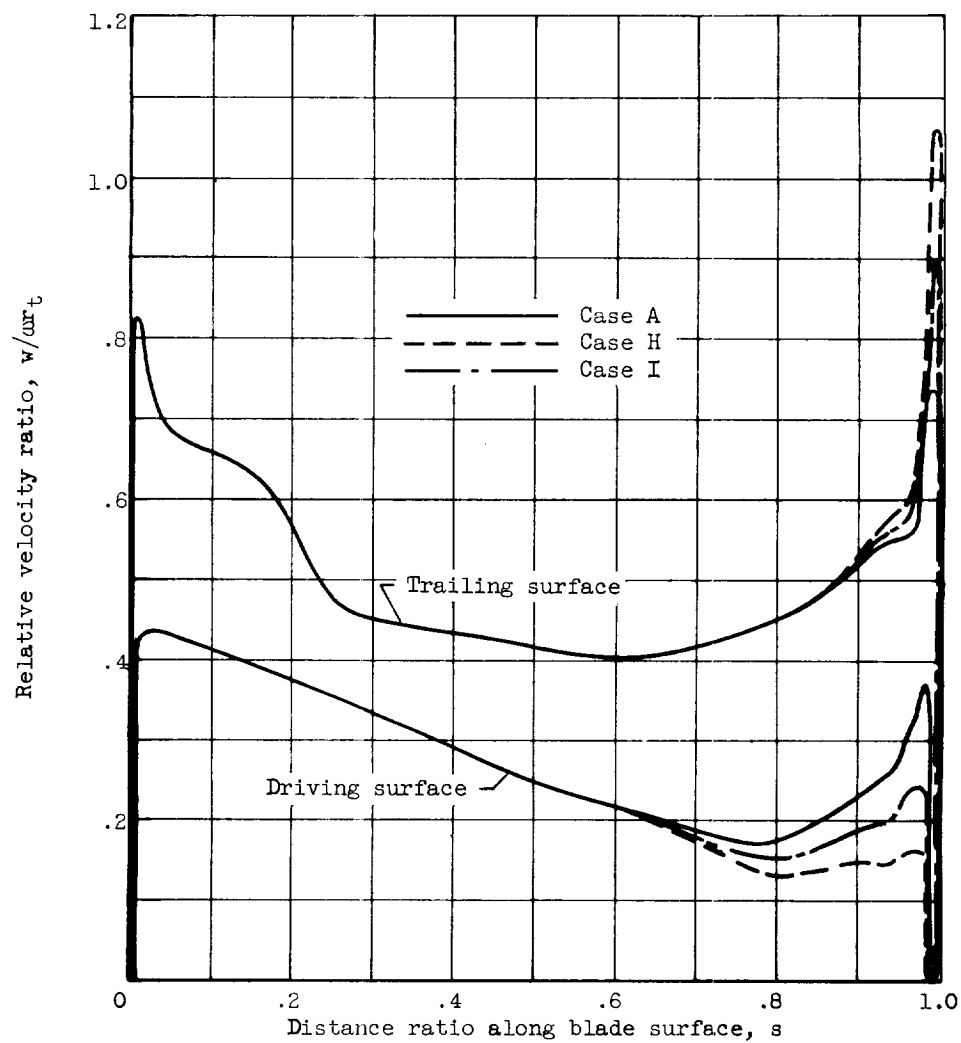


Figure 8. - Distribution of relative velocity ratio along blade surface showing effect of varying the downstream boundary conditions (location of stagnation point or slip factor).

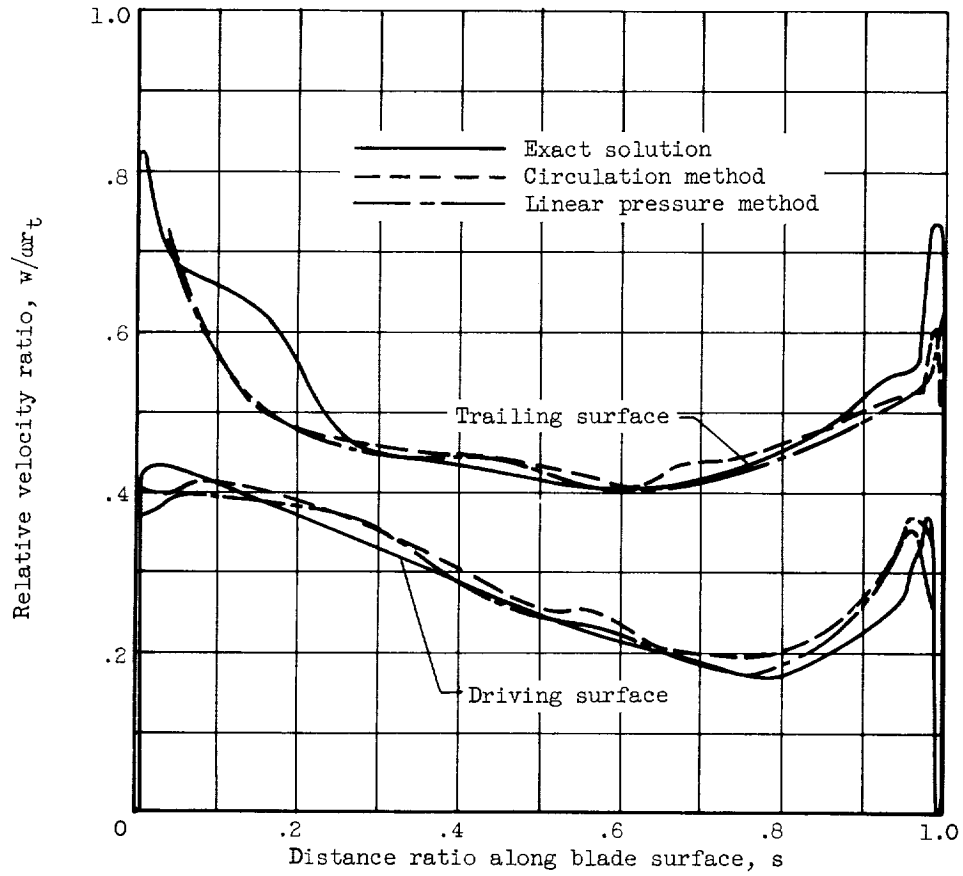


Figure 9. - Comparison of two approximate methods of obtaining blade surface velocities with exact solution for case A; $\alpha = 0^\circ$.

E-816

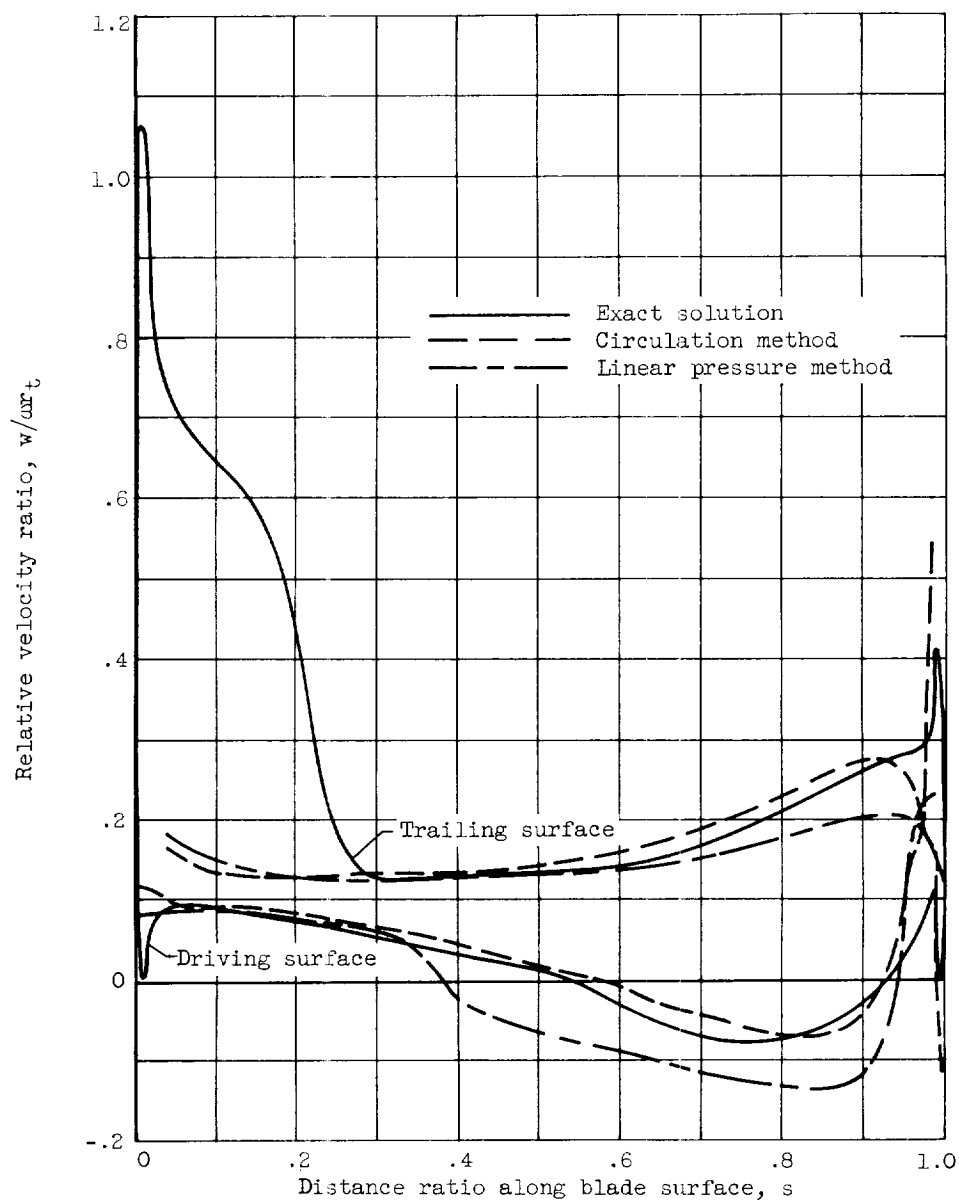


Figure 10. - Comparison of two approximate methods of obtaining blade surface velocities with exact solution for case D with eddy; $\alpha = 5^\circ$.

